Nanoscale Res Lett (2008) 3:330–337
DOI 10.1007/s11671-008-9161-1

NANO EXPRESS

Synthesis, Electrical Measurement, and Field Emission Properties of α-Fe_2O_3 Nanowires

Li-Chieh Hsu · Yuan-Yao Li · Chun-Yen Hsiao

Received: 26 June 2008 / Accepted: 18 August 2008 / Published online: 9 September 2008

Abstract α-Fe_2O_3 nanowires (NWs) were formed by the thermal oxidation of an iron film in air at 350 °C for 10 h. The rhombohedral structure of the α-Fe_2O_3 NWs was grown vertically on the substrate with diameters of 8–25 nm and lengths of several hundred nm. It was found that the population density of the NWs per unit area (D_{NWs}) can be varied by the film thickness. The thicker the iron film, the more NWs were grown. The growth mechanism of the NWs is suggested to be a combination effect of the thermal oxidation rate, defects on the film, and selective directional growth. The electrical resistivity of a single NW with a length of 800 nm and a diameter of 15 nm was measured to be 4.42×10^3 Ωcm using conductive atomic force microscopy. The field emission characteristics of the NWs were studied using a two-parallel-plate system. A low turn–on field of 3.3 V/μm and a large current density of 10^{-3} A/cm^2 (under an applied field of about 7 V/μm) can be obtained using optimal factors of D_{NWs} in the cathode.

Keywords Nanowires · Field emission · Conductive atomic force microscopy (CAFM)

Introduction

One-dimensional (1D) nanostructures have been extensively studied because of their unique chemical and physical characteristics. Because of their high aspect ratio and sharp tips that enhance the local electrical field, they can be used as emitters in field emission (FE) applications [1]. Factors that affect FE properties include the population density of the emitters (the number of emitters per unit square) [2], the electronic resistance of a single emitter [3], and the aspect ratio (radius and length) [4]. The field emission properties of an emitter are affected by nearby emitters, which is called the field screen effect. Many research groups have studied the relationship between FE properties (field screen effect) and the population density of emitters for ZnO nanowires (NWs) [5], Si NWs [6], CNTs [2, 3], and CuO NWs [1]. Poor FE properties were obtained when the population density of the emitters was too high.

Investigating the electronic properties of 1D nanomaterials can reveal the relationship between the electronic properties of emitters and the FE properties of the device. In addition, it can provide useful information for the theoretical study of FE characteristics. Electronic measurement methods for NWs are generally categorized into four types: (1) laterally growing NWs between two electrodes and directly measuring them [7, 8], (2) spreading the NWs on a large number of patterned electrodes and measuring a single NW on a pair of electrodes [9, 10], (3) directly measuring vertical NWs using conductive atomic force microscopy (CAFM) [11, 12], and (4) measuring aligned NWs arrays using two electrode films [13, 14]. The CAFM system is a convenient method for the non-destructive characterization of the electronic properties of NWs.

α-Fe_2O_3 (hematite) is a semiconductor (Eg = 2.1 eV) and the most stable iron oxide under an ambient environment [15]. α-Fe_2O_3 NWs have recently been synthesized by various research groups [16, 17]. Because they are

L.-C. Hsu · Y.-Y. Li (✉)
Department of Chemical Engineering, National Chung Cheng University, 168 University Rd, Min-Hsiung, Chia-Yi 621, Taiwan, R.O.C
e-mail: chmyyl@ccu.edu.tw

C.-Y. Hsiao
TECO Nanotech Co. Ltd, Taoyuan 328, Taiwan, R.O.C

thermally stable, resistant to oxidation, and have a high aspect ratio, α-Fe_2O_3 NWs are a candidate emitters for FE applications. It has been reported that an electrical field of 7–8 V/μm is required to obtain a 10^{-5} A/cm^2 emission current using densely packed α-Fe_2O_3 NWs as emitters [16]. However, there have been no detailed studies on FE properties related to the population density of α-Fe_2O_3 NWs (D_{NWs}) and their resistance (R_{NW}).

In this study, we report a simple method that can be used to control the population density of α-Fe_2O_3 NWs (D_{NWs}) by varying the film thickness of iron. The FE properties of α-Fe_2O_3 NWs with various population densities and resistances (R_{NW}) were studied. It was found that the best FE properties can be obtained by using the optimal D_{NWs} in the cathode.

Experimental Details

α–Fe_2O_3 NWs were grown using an iron film thermally oxidized at 350 °C for 10 h. Iron films with thicknesses of 30 nm, 50 nm, 100 nm, and 150 nm were coated on indium tin oxide (ITO) glass by direct current (DC) sputtering. The iron-coated substrates were heated at 350 °C for 10 h in an oven in the air atmosphere. The morphology and crystalline structure of the as-synthesized NWs were characterized by field emission scanning electron microscopy (FE-SEM, HITACH S-4800) and high-resolution transmission electron microscopy (HR-TEM, JEOL JSM 3010), respectively. The current–voltage (I–V) characteristics of the as-grown NWs were obtained using the CAFM (SEIKO SPA-400) system. A highly conductive polygon shaped tip with a height of 10 μm and a radius of 50 nm (the top of the tip) was used as an electronic probe while ITO was used as an electrode. The applied voltages were −10 V to +10 V. FE properties were measured in a vacuum chamber at 6×10^{-6} torr. The sweep voltage was 0–1100 V and the emission current was measured using Keithley 2410.

Results and Discussion

Figure 1a and b shows the top view and cross-section view of the Fe-coated (50 nm) ITO glass after thermal oxidation at 350 °C for 10 h, respectively. As can be seen in Fig. 1a, the NWs formed randomly on the film. Figure 1b shows that the NWs were grown vertically on the film with diameters of 8–25 nm and lengths of several hundred nm. Fe film was oxidized during the process and became α-Fe_2O_3 film with a thickness of 100 nm.

Figure 2 shows the TEM images of an α-Fe_2O_3 NW which was grown on the iron film with a thickness of

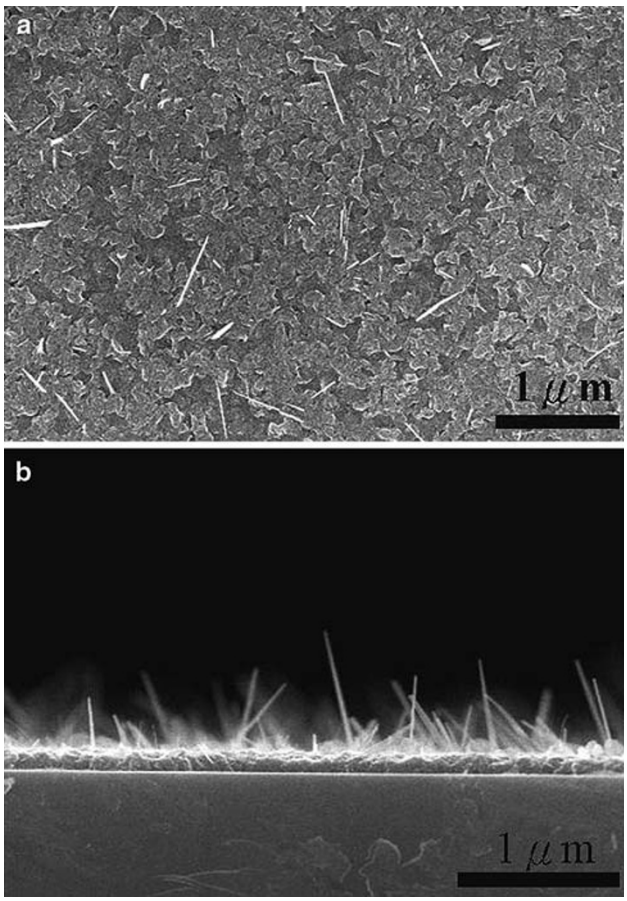

Fig. 1 FE-SEM images of (**a**) the top view and (**b**) cross-section view of NWs synthesized on Fe-coated (50 nm) ITO glass at 350 °C for 10 h

50 nm. As can be seen in Fig. 2a, the length and diameter of the as-produced α-Fe_2O_3 NWs were approximately 240 nm and 25 nm, respectively. Figure 2b shows the high-resolution TEM image and its corresponding selective area electron diffraction (SAED) pattern (inset). It was found that the NW is a single crystalline α-Fe_2O_3 NW with the [110] growth direction. The interplanar spacing of 0.251 nm agrees well with the fringe spacing of α-Fe_2O_3. The SAED pattern reveals that the crystal structure of the α-Fe_2O_3 NW is rhombohedral.

The length, diameter, and population density of the α-Fe_2O_3 NWs were studied for various Fe film thicknesses. Samples A, B, C, and D represent the materials after the thermal oxidation of the 30 nm, 50 nm, 100 nm, and 150 nm-thick iron films, respectively. Figure 3a–d shows the top views of sample A (30 nm), sample B (50 nm), sample C (100 nm), and sample D (150 nm), respectively. As can be seen, the number of α-Fe_2O_3 NWs increased with an increase of the film thickness. D_{NWs} was calculated from the SEM image as 1.6×10^8 NWs/cm^2 for sample A, 7.8×10^8 NWs/cm^2 for sample B, 13.2×10^8 NWs/cm^2

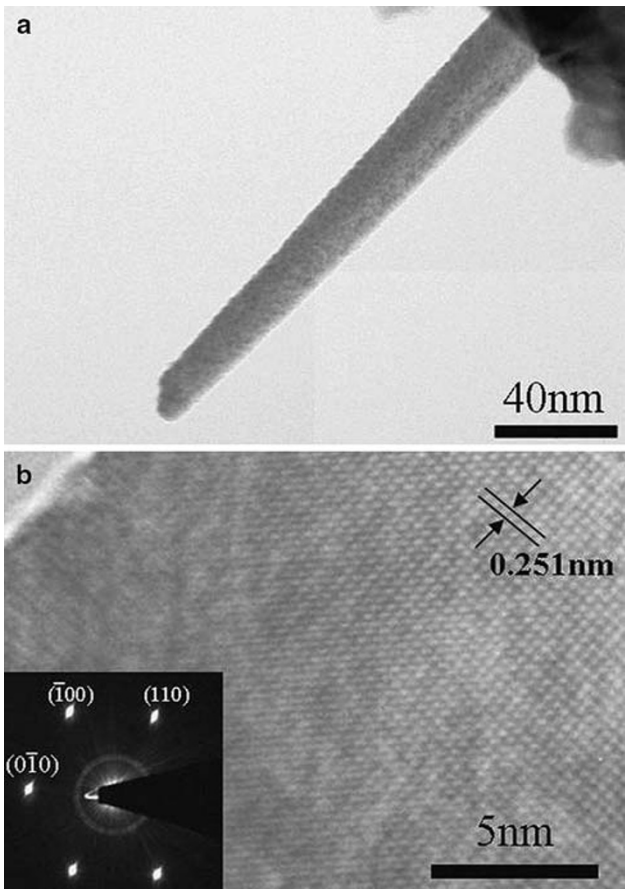

Fig. 2 (**a**) TEM image of an α-Fe_2O_3 NW, (**b**) HR-TEM image of the α-Fe_2O_3 nanowire, and the SAED pattern of the α-Fe_2O_3 NW (inset)

for sample C, and 18.3 × 10^8 NWs/cm^2 for sample D. Table 1 summarizes the population densities of the samples. Figure 3e shows a plot of NW density (D_{NWs}) versus iron film thickness. The error in the D_{NWs} measurements is about 5%.

The growth mechanism of the α-Fe_2O_3 NWs via thermal oxidation was discussed by Takagi [18] and Fu et al. [19]. They proposed that the growth mechanism of the α-Fe_2O_3 NWs was neither vapor–liquid–solid (VLS) nor vapor–solid (VS). A tip growth mechanism was suggested, in which the NWs are grown by the diffusion of oxygen atoms on the surface defects of the iron film. During the thermal process, the oxygen molecules diffuse into the iron film between the iron atoms and form Fe–O bonds. The process involves a volume expansion in all three dimensions to accommodate the oxygen atoms. However, because the iron film prevents expansion in the two lateral directions, the volume of oxides expands upward only. A thin oxide film is therefore formed on the substrate. While a layer of the oxide forms, defects are created in the oxide film. This might be caused by a rapid thermal oxidation rate on the surface of the film during the temperature ramping period. The defects can be seen as crackings on the surface of the film (Fig. 1a). As the oxidation time increases, in regions with a higher degree of defects, the oxygen molecules move faster, diffuse across the existing oxide layer, and react with iron to form iron oxide. There was an oxidation rate difference (growth rate of α-Fe_2O_3 NWs) between the high degree and low degree defect regions. In addition, the preferred growth orientation of α-Fe_2O_3 NWs was the [110] direction (Fig. 2b), which suggests that the fastest growth rate was along the [110] direction. Therefore, the oxidation rate difference and the selective directional growth are probable reasons for the formation of α-Fe_2O_3 NWs. A schematic graph of the formation of α-Fe_2O_3 NWs is shown in Fig. 4. Samples I and II represent the thin and thick iron films, respectively. After oxidation for a period of time (stage A), the thin iron film (sample I) was completely oxidized to become α-Fe_2O_3 NWs and α-Fe_2O_3 film. In contrast, the thick iron film was partially oxidized so that α-Fe_2O_3 NWs, α-Fe_2O_3 film, and Fe film were present in stage I. At this stage, for both samples I and II, short NWs (<100 nm) and long NWs (>500 nm) grew from the low and high degree defect regions of the film, respectively. As the oxidation time increased (stage B), the length and D_{NWs} of sample I did not change because the oxidation terminated at stage A. For sample II, the oxidation continued; NWs were continuously grown, becoming longer and more dense. Takagi [18] observed that the population density and the length of NWs were dependent of the oxidation time. Our results show good agreement with Takagi's report. The population density of NWs can be increased by increasing the thickness of the iron film.

CAFM was employed to measure the electronic property of a single α-Fe_2O_3 NW and α-Fe_2O_3 film. Figure 5a shows the schematic drawing of the CAFM measurement. NWs were embedded in photoresist (PR) and only the tips of the NWs (sample B) were exposed. The CAFM tip made contact with the exposed tips of the NWs so that their electronic properties could be measured. Using PR prevented the bending of the NWs while the CAFM tip approached them. The applied voltage was swept from −10 V to +10 V to obtain the I–V characteristics for a single NW. The equivalent circuit diagram for the measurement of an α-Fe_2O_3 NW is shown in Fig. 5b. $R_{contact}$ is the contact resistance between the CAFM tip and the NW. R_{NW} and R_{film} are the resistances of the NW and the film, respectively. The overall resistance ($R_{overall}$) is the sum of $R_{contact}$, R_{NW}, and R_{film}. It can be expressed as:

$$R_{overall} = R_{contact} + R_{NW} + R_{film}. \quad (1)$$

Figure 5c shows the top view and side view (inset) of a sample. As can be seen, a single NW with a diameter of 15 nm and a length of 800 nm was embedded in the PR.

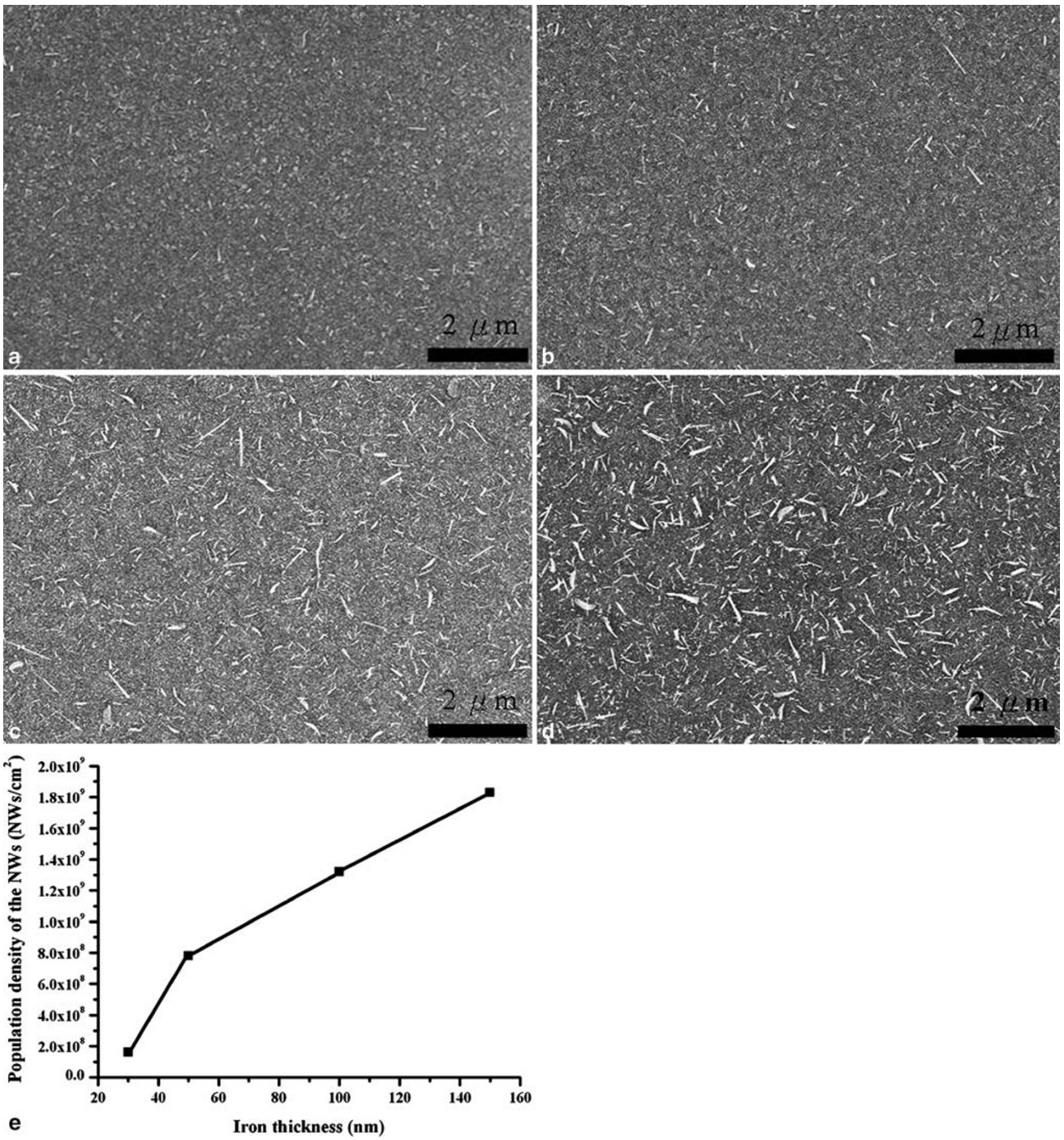

Fig. 3 FE-SEM images of α-Fe_2O_3 NWs grown on (**a**) 30 nm, (**b**) 50 nm, (**c**) 100 nm, and (**d**) 150 nm iron films, and (**e**) the population density of α-Fe_2O_3 NWs as a function of the film thickness

Only the tip of the NW was exposed on the PR surface. The figure also shows that the NWs were not bent or damaged after the spin coating process of the PR. Figure 6a and b shows the morphology image and current image, respectively, taken at a +10 V bias on a single NW. The tip used for CAFM was an Au-coated silicon tip, with a diameter of about 50 nm. The morphology image of the NW shows that the diameter of the NW was larger than that observed by SEM, which was due to the large diameter of the scanning tip. From the current image taken at a +10 V bias, the bright zone indicates that a current appeared on the tip of the single NW. It can also be seen that there was no current

Table 1 Summary of the population densities (D_{NWs}), resistances of NWs (R_{NW}), turn–on field (E_{to}), and calculated field enhancement factors (β) for samples A, B, C, and D

Sample	Iron thickness (nm)	Population density of the NWs (D_{NWs}) (NWs/cm^2)[a]	Resistance of a NM(R_{NW})(Ω)	Turn-on field (E_{to}) (V/μm)	Field enhancement factor(β)	R_{total}(Ω) of NEs[b]
A	30	1.6×10^8	1.25×10^{11}	4.3	1023	781
B	50	7.8×10^8	2×10^{11}	3.3	1754	256
C	100	1.32×10^9	1.4×10^{11}	4.5	1434	106
D	150	1.83×10^9	6.25×10^{10}	4.7	1420	34

[a] The popular density of the NWs per cm^2

[b] R_{total}: the resistance of the total NWs in a unit cm^2

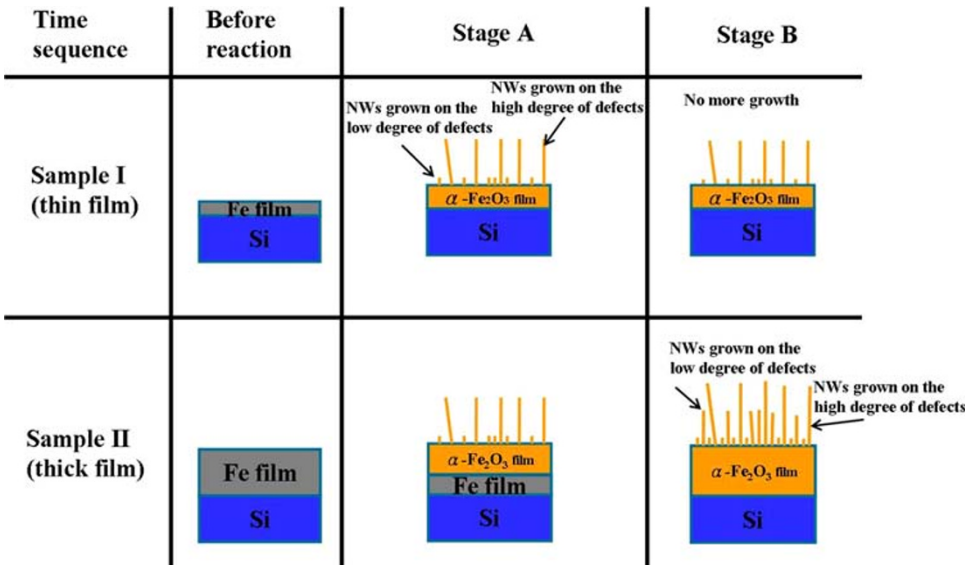

Fig. 4 A schematic graph of the formation of the α-Fe_2O_3 NWs in thin and thick iron

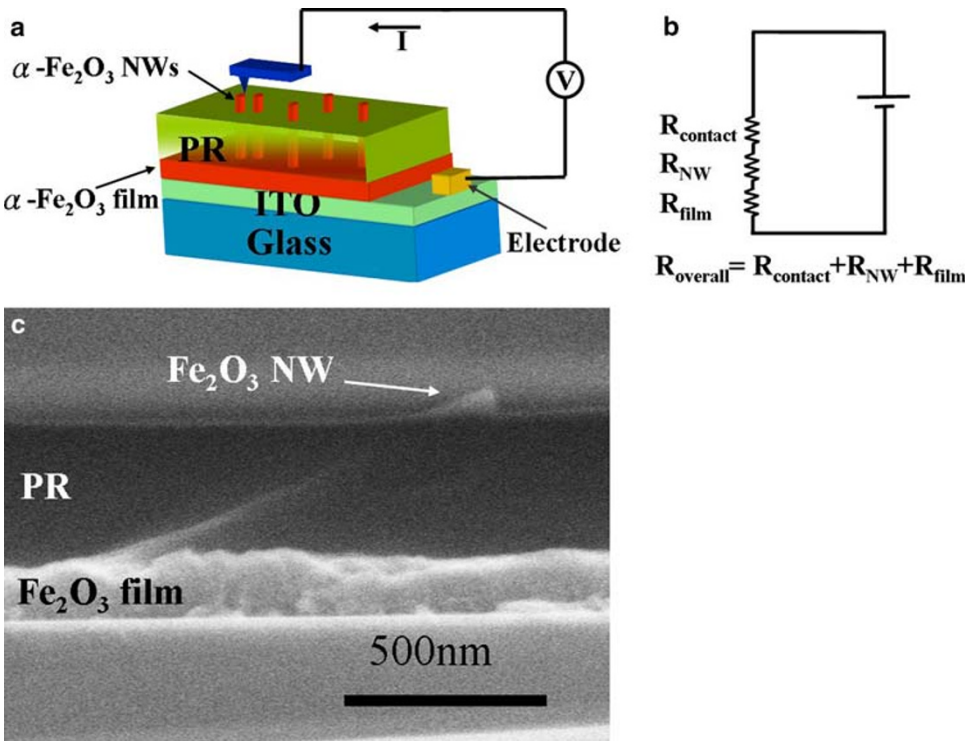

Fig. 5 (**a**) Schematic illustration and (**b**) circuit diagram of conductive atomic force microscopy. (**c**) Top-view and side-view (inset) FE-SEM images of the embedded NWs

signal in the PR region. Figure 7 shows the I–V curves of the structure of the ITO/α-Fe_2O_3 film/α-Fe_2O_3 NW/CAFM-tip (Fig. 7a) and the ITO/α-Fe_2O_3 film/ CAFM-tip (Fig. 7b). Nanowires from sample B were removed by ultrasonication in ethanol. The bias voltage was swept from −10 V to +10 V. The measured resistances of the ITO/α-Fe_2O_3 film/α-Fe_2O_3 NW/CAFM-tip structure ($R_{overall}$) and the ITO/α-Fe_2O_3 film/CAFM-tip structure (indicated as $R_{film} + R_{contact}$) were 2×10^{11} Ω and 4.2×10^9 Ω, respectively. Because $R_{film} + R_{contact}$ (4.2×10^9 Ω) was much smaller than $R_{overall}$ (2×10^{11} Ω) and $R_{contact}$ is considered to be much smaller than R_{NW} and R_{film}, Eq. 1 can be rewritten as:

$$R_{overall} \approx R_{NW}. \quad (2)$$

In other words, the resistance of the ITO/α-Fe_2O_3 film/α-Fe_2O_3 NW/CAFM-tip structure ($R_{overall}$) can be considered as R_{NW}. R_{NW} can be expressed as:

$$R_{NW} = \rho \frac{L}{\pi r^2}, \quad (3)$$

where ρ is the electronic resistivity of an α-Fe_2O_3 NW, and L and r represent the average length (800 nm) and radius (15 nm) of the NW, respectively. We assumed that ρ (4.42×10^3 Ωcm) is a constant for all of the as-produced α-Fe_2O_3 NWs. Using the mean length and radius of the NWs, R_{NW} (or $R_{overall}$) of samples A, B, C, and D was calculated as 1.25×10^{11}, 1.4×10^{11}, 1.4×10^{11}, and 6.25×10^{10} Ω, respectively. The values are shown in Table 1.

The two-parallel-plate system used for FE measurement is shown in Fig. 8a. The cathode consisted of the α-Fe_2O_3

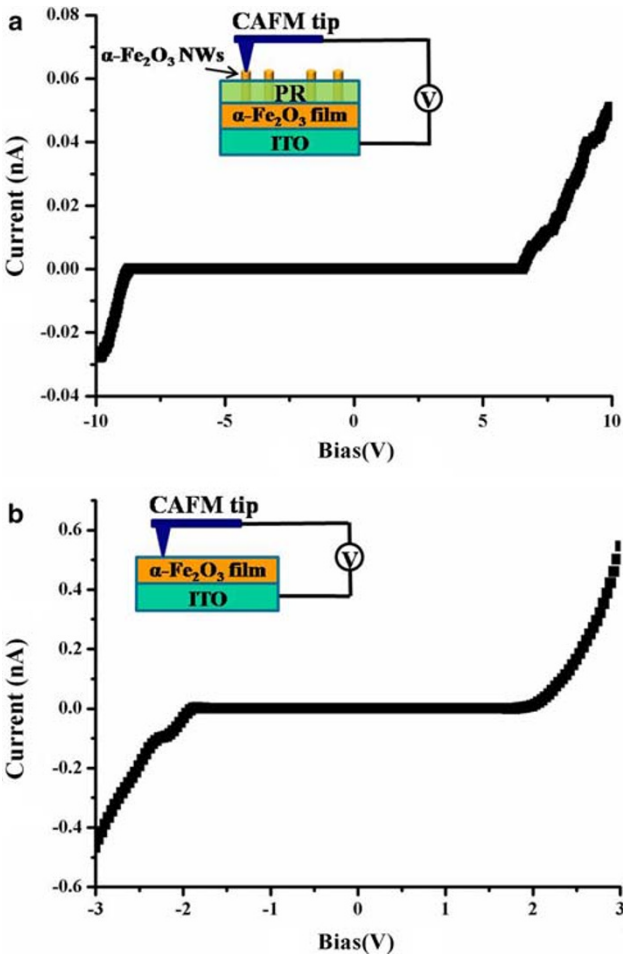

Fig. 7 The I–V characteristics of (**a**) the ITO/α-Fe_2O_3 film/α-Fe_2O_3 NW/CAFM-tip structure and (**b**) the ITO/α-Fe_2O_3 film /CAFM-tip structure

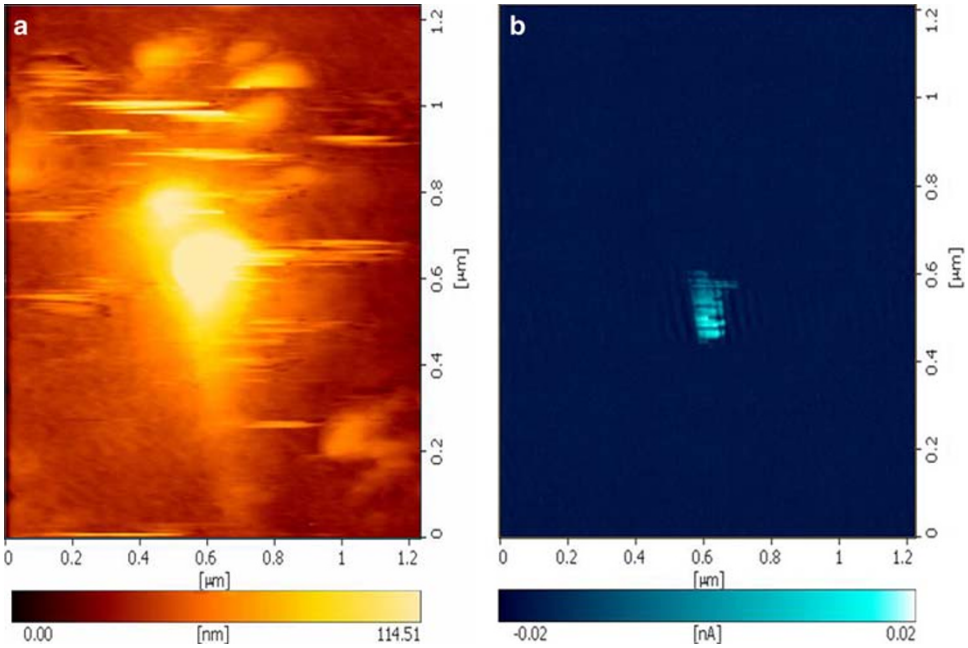

Fig. 6 The CAFM images of (**a**) morphology and (**b**) current taken at a +10 V bias

emitters, α-Fe_2O_3 film, and ITO glass while the anode was ITO glass. The cathode and anode were separated by a 150 μm-thick spacer. Figure 8b shows the curve of the field emission current density versus electrical field (J-E) for the four samples. The turn-on field (E_{to}) is defined as the value of the applied electrical field which produces an emission current density of 10 μA/cm^2. To analyze the field emission properties of α-Fe_2O_3 NWs, the Fowler-Nordheim (F-N) [20] equation was used. The equation can be expressed as:

$$J = A\frac{(\beta F)^2}{\varphi}\mathrm{e}^{\left(\frac{-B\varphi^{3/2}}{\beta F}\right)}, \quad (4)$$

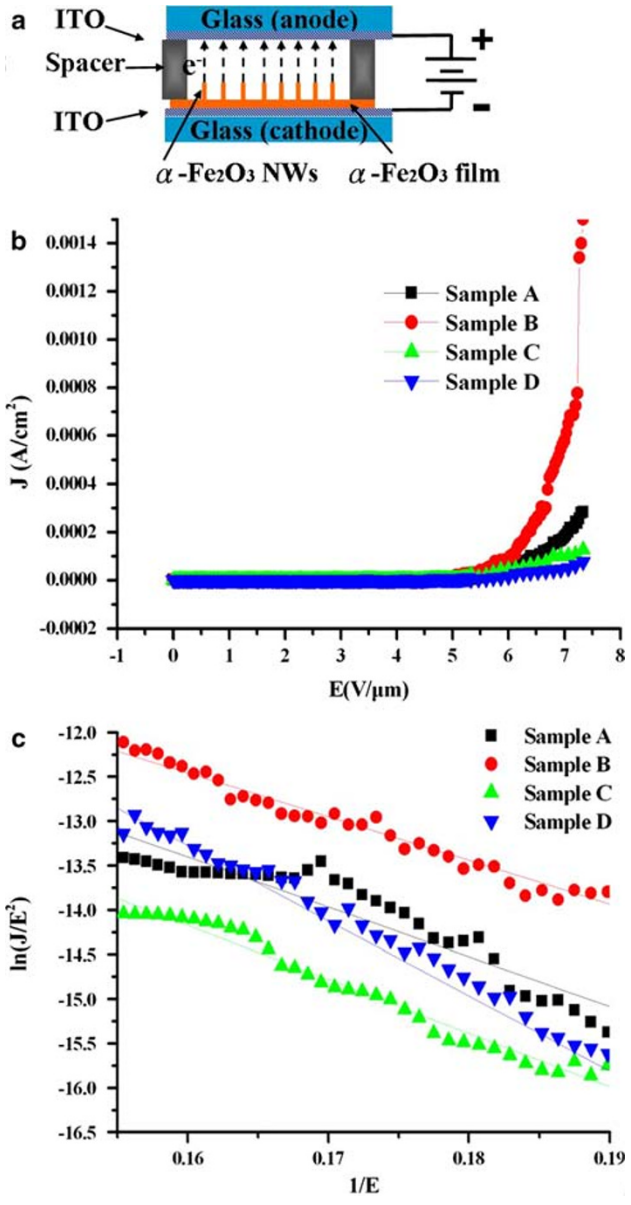

Fig. 8 (**a**) Illustration of the two-parallel-plate configuration used for field emission (FE) measurement, (**b**) the current density as a function of the electrical field for the four samples, and (**c**) the F–N plot

where J is the emission current density; φ is the work function; F is the electrical field; $A = 1.54 \times 10^{-6}$ AeVV^{-2}; $B = 6.83 \times 10^3$ eV$^{-3/2}$ Vμm^{-1}, and β is the field enhancement factor. β is a parameter that depends on the crystal structure and the morphology of the emitters. The work function of α-Fe_2O_3 is 5.6 eV [16], so β can be calculated as 1023, 1754, 1434, and 1420 for samples A, B, C, and D, respectively. Figure 8c shows the Fowler-Nordheim (F-N) plot of the four samples. The linear relationship of $1/E$ and $\ln(J/E^2)$ indicates that the field emission behavior of the samples fits the F-N mechanism. Table 1 summarizes the results of the turn-on field and field enhancement factor (β). Emitters with D_{NWs} of 7.8×10^8 NWs/cm^2 (sample B) showed the lowest E_{to} and the highest β in our study. Sample B had a medium population density of the α-Fe_2O_3 emitters. In contrast, emitters with low D_{NWs} (sample A) showed the lowest β and a "modest" E_{to} due to insufficient emission sites.[3] Densely packed NWs (samples C and D) caused the screen effect[21], leading to field emission performance that was not as good as that of sample B. Compared to other 1D materials, such as ZnO NWs, [5] Si NWs, [6] CNTs [2, 3], and CuO NWs, [1] NWs with high β and low E_{to} can be achieved by controlling their population density. Our study agrees well with other studies.

The relationship between the field enhancement factor (β), resistance of α-Fe_2O_3 NWs (R_{NW}), and the population density (D_{NWs}) of the four samples was analyzed; it is shown in Fig. 9. R_{NW} of samples A, B, C, and D are similar, but β is different for each sample. According to the results, the value of β depends on D_{NW} more than it does on R_{NW}. Bonard et al. [21] observed that β depends on D_{NW} more than it does on the length of CNT. The length of CNT increased with an increase in resistance. Our results show good agreement with Bonard's research.

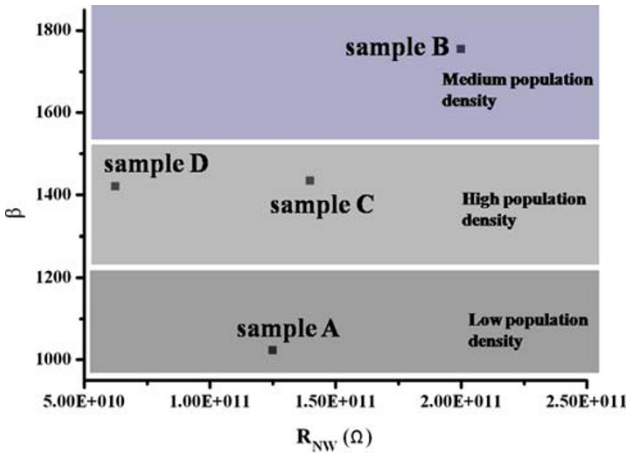

Fig. 9 The field enhancement factor (β) and resistance of NWs (R_{NW}) as a function of the turn-on field (E_{to})

Conclusion

The formation, electronic characterization, and field emission application of α-Fe_2O_3 NWs were studied. α-Fe_2O_3 NWs were grown vertically on the substrate via the thermal oxidation of an iron film in air at 350 °C for 10 h. By increasing the film thickness (to 30, 50, 100, and 150 nm), D_{NWs} could be increased. R_{NW} of the NWs was estimated using the CAFM technique. In the FE study, an E_{to} of 3.3 V/μm and a large current density of 10^{-3} A/cm^2 (under an applied field of about 7 V/μm) were obtained with the optimum D_{NWs}. The densely packed NWs caused the screen effect, leading to poor FE performance. The field enhancement factor (β) depends on D_{NW} more than it does on R_{NW}. This study shows that α-Fe_2O_3 NWs are a candidate for emitters in field emission applications.

Acknowledgments The authors would like to thank Mr. Shu-Teng Chou at Advantage Scientific Incorporated for his help in CAFM measurements. Mr. Chien-Wei Huang at National Chung Cheng University is acknowledged for his help in sputtering iron films.

References

1. Y.W. Zhu, T. Yu, F.C. Cheong, X.J. Xui, C.T. Lim, V.B.C. Tan et al., Large-scale synthesis and field emission properties of vertically oriented CuO nanowire films. Nanotechnology **16**, 88–92 (2005). doi:10.1088/0957-4484/16/1/018
2. L. Nilsson, O. Groening, C. Emmenegger, O. Kuettel, E. Schaller, L. Schlapbach et al., Scanning field emission from patterned carbon nanotube films. Appl. Phys. Lett. **76**, 2071–2073 (2000). doi:10.1063/1.126258
3. H. Gao, C. Mu, F. Wang, D.S. Xu, K. Wu, Y.C. Xie et al., Field emission of large-area and graphitized carbon nanotube array on anodic aluminum oxide template. J. Appl. Phys. **93**, 5602–5605 (2003). doi:10.1063/1.1564882
4. J.M. Bonard, M. Croci, I. Arfaoui, O. Noury, D. Sarangi, A. Chatelain, Can we reliably estimate the emission field and field enhancement factor of carbon nanotube film field emitters? Diam. Relat. Mater. **11**, 763–768 (2002). doi:10.1016/S0925-9635(01)00541-6
5. S.H. Jo, J.Y. Lao, Z.F. Ren, R.A. Farrer, T. Baldacchini, J.T. Fourkas, Field-emission studies on thin films of zinc oxide nanowires. Appl. Phys. Lett. **83**, 4821–4823 (2003). doi:10.1063/1.1631735
6. B.Q. Zeng, G.Y. Xiong, S. Chen, W.Z. Wang, D.Z. Wang, Z.F. Ren, Field emission of silicon nanowires grown on carbon cloth. Appl. Phys. Lett. **90**, 033112-1–033112-3 (2007)
7. J. Kim, W.A. Anderson, Direct electrical measurement of the self-assembled nickel silicide nanowire. Nano Lett. **6**, 1356–1359 (2006). doi:10.1021/nl0602894
8. J.S. Lee, M.S. Islam, S. Kim, Direct formation of catalyst-free ZnO nanobridge devices on an etched Si substrate using a thermal evaporation method. Nano Lett. **6**, 1487–1490 (2006). doi:10.1021/nl060883d
9. F. Hernandez-Ramirez, A. Tarancon, O. Casals, E. Pellicer, J. Rodriguez, A. Romano-Rodriguez et al., Electrical properties of individual tin oxide nanowires contacted to platinum electrodes. Phys. Rev. B **76**, 085429–085433 (2007). doi:10.1103/PhysRevB.76.085429
10. H.K. Seong, J.Y. Kim, J.J. Kim, S.C. Lee, S.R. Kim, U. Kim et al., Room-temperature ferromagnetism in cu doped GaN nanomores. Nano Lett. **7**, 3366–3371 (2007). doi:10.1021/nl0716552
11. M. Nebeschutz, V. Cimalla, O. Ambacher, T. Machleidt, J. Ristic, E. Calleja, Electrical performance of gallium nitride nanocolumns. Physica E **37**, 200–203 (2007). doi:10.1016/j.physe.2006.10.007
12. E. Schlenker, A. Bakin, B. Postels, A.C. Mofor, H.H. Wehmann, T. Weimann et al., Electrical characterization of ZnO nanorods. Physica E **244**, 1473–1477 (2007)
13. A.O. Adeyeye, R.L. White, Magnetoresistance behavior of single castellated Ni80Fe20 nanowires. J. Appl. Phys. **95**, 2025–2028 (2004). doi:10.1063/1.1637726
14. I. Liu, Y.H. Wu, H.H. Long, Z.J. Liu, Y.K. Zheng, A.O. Adeyeye, Transport properties and micromagnetic modeling of magnetic nanowires with multiple constrictions. Thin Solid Films **505**, 35–40 (2006). doi:10.1016/j.tsf.2005.10.034
15. R. Dieckmann, Point-defects and transport in hematite (Fe2o3-Epsilon). Philos. Mag. A **68**, 725–745 (1993). doi:10.1080/01418619308213994
16. Y.L. Chueh, M.W. Lai, J.Q. Liang, L.J. Chou, Z.L. Wang, Systematic study of the growth of aligned arrays of alpha-Fe2O3 and Fe3O4 nanowires by a vapor-solid process. Adv. Funct. Mater. **16**, 2243–2251 (2006). doi:10.1002/adfm.200600499
17. L.-C. Hsu, Y.-Y. Li, C.G. Lo, C.W. Huang, G. Chern, Thermal growth and magnetic characterization of the α-Fe2O3 nanowires. J. Phys. D Appl. Phys. (2008) (accepted)
18. R. Takagi, J. Phys. Soc. Jpn. **12**, 1212–1218 (1957). doi:10.1143/JPSJ.12.1212
19. Y.Y. Fu, R.M. Wang, J. Xu, J. Chen, Y. Yan, A. Narlikar et al., Synthesis of large arrays of aligned alpha-Fe2O3 nanowires. Chem. Phys. Lett. **379**, 373–379 (2003). doi:10.1016/j.cplett.2003.08.061
20. R.E. Burgess, H. Kroemer, J.M. Houston, Corrected values of Fowler-Nordheim field emission functions V(Y) and S(Y). Phys. Rev. **90**, 515–515 (1953). doi:10.1103/PhysRev.90.515
21. J.M. Bonard, N. Weiss, H. Kind, T. Stockli, L. Forro, K. Kern et al., Tuning the field emission properties of patterned carbon nanotube films. Adv. Mater. **13**, 184–188 (2001). doi :10.1002/1521-4095(200102)13:3<184::AID-ADMA184>3.0.CO;2-I